RESEARCH ARTICLE | Full Access

Nitrogen Fixation Through Al_2O_3–Based Catalysts Embedded in a Microwave Plasma Post–Discharge

Babak Sadeghi, Rony Snyders, Marie–Paule Delplancke

First published: 09 February 2026 | https://doi.org/10.1002/ppap.70136 | VIEW METRICS

ABSTRACT

The conventional Haber–Bosch process for nitrogen fixation is energy-intensive and associated with high greenhouse gas emissions. Plasma-assisted catalysis represents an alternative approach for nitrogen oxidation under milder conditions. In this study, catalyst-assisted microwave plasma was investigated using alumina-based catalysts and alumina-supported metal oxides (Mo, W, Co, and Ni). Microwave plasma alone predominantly produced NO, whereas the presence of catalysts promoted additional NO_2 formation, indicating the importance of plasma–catalyst interactions. Catalytic performance depended strongly on the physicochemical properties of alumina, with δ-Al_2O_3 exhibiting the highest activity. Mo- and W-loaded catalysts further enhanced NO_x formation, while Ni and Co showed weaker effects. An overall increase of up to ~30% in NO_x production was achieved compared to plasma alone.

1 Introduction

Nitrogen is an essential component of all living organisms and a basic element for synthesizing many chemical products [1-6]. However, N_2, which is the main constituent of our atmosphere, is chemically inert and is inaccessible to most organisms in its original form. Therefore, to be utilized, it must be first converted into other more reactive forms like ammonia or nitrates in a process named "NF." The natural processes allowing NF are mostly lightning and the activity of some bacteria [7, 8]. Since the industrialization of agriculture became necessary in view of the demand for food due to global population growth, the utilization of nitrogen-based fertilizers has driven the development of artificial NF processes [9]. Therefore, during the first decade of the 20th century, intensive research efforts led to the development of several industrial NF processes. The three most interesting processes that have been developed are (i) the direct combination of nitrogen with oxygen in an electric arc (Birkeland-Eyde process, B–E), (ii) the reaction of nitrogen with calcium carbide (Frank-Carlo process, F–C), at a high temperature to form calcium cyanamide, which is hydrolyzed to ammonia and urea and (iii) the synthesis of NH_3 with the catalytic reaction between H_2 and N_2 (Haber-Bosch process, H–B) [10-12]. Because of too high energy-cost, the B–E and F–C processes have quickly been replaced by the H-B process which is still the dominant approach [10]. In the H–B process, N_2 is combined with H_2 under extremely high pressures (100–250 bar) and moderately elevated temperatures (500°C) in the presence of an active catalyst (Fe or Ru-based catalysts) to yield a high proportion of ammonia [12]. For a fully optimized and integrated H-B process, an energy efficiency as low as 0.48 MJ mol^{-1} of nitrogen is reported [13, 14]. Nevertheless, despite this reliable performance, this process consumes almost 1%–2% of the world's total energy, emitting more than 300 million tons of carbon dioxide annually [15]. In addition, a fully operational H–B process demands a large infrastructure that does not allow for decentralization on a small scale which makes the transportation requirement an additional disadvantage of this method [15]. It is therefore necessary to develop new NF processes that allow for lower energy costs and present a lower impact on the environment [16-19].

In this context, plasma-based processes, which are electrically driven processes (i.e., green method and fast responding), have gained a great deal of attention from NF. The plasma-based NO_x formation has been studied in many kinds of plasmas starting from the oldest B–E process to the lastly developed gliding arc plasmas [20-27]. Indeed, plasmas are reported as one of the promising approaches for the activation of the N_2 bond as it denotes a reactive environment due to the presence of charges, excited species, and radicals [28, 29]. Recently, the importance of reactive species like atomic and molecular excitations of nitrogen and oxygen has been studied and discussed for NO_x formation under various plasma environments [21, 30]. Literature suggests that vibrationally excited N_2 molecules play a key role in N_2 fixation processes which can provide better energy efficiency for endothermic chemical reactions in non-equilibrium conditions [21, 28, 29, 31]. Till now, non-thermal microwave plasma (MWP) with a magnetic field (electron cyclotron resonance) presented the

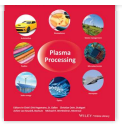

February 2026
e70136

Figures | References | Related | Information

Recommended

Microplasma for Nitrogen Fixation
Liangliang Lin
Plasma-Assisted Nitrogen Fixation for Sustainable Process Industries, [1]

Regulation of nitrogen fixation in *Azospirillum brasilense*
Yaoping Zhang, Robert H Burris, Paul W Ludden, Gary P Roberts
FEMS Microbiology Letters

Transfer of Nitrogen Fixation (*nif*) Genes to Non-diazotrophic Hosts
Qin Li, Sanfeng Chen
ChemBioChem

Optimization of Polyethersulfone Surface Properties Using Plasma Treatment Generated by Diffuse Coplanar Surface Barrier Discharge
Pedram Ghourchi Beigi, Leila Zahedi, Monika Stupavská, František Zažímal, Petra Šrámková, Tomáš Homola, Dušan Kováčik
Plasma Processes and Polymers

Decomposition of CO_2 by Bubbling It Through a Microwave Discharge in Liquid Ethanol
Timur S. Batukaev, Igor V. Bilera, Galina V. Krashevskaya, Yuri A. Lebedev, Kristina V. Smirnova, Vladislav K. Shumilov
Plasma Processes and Polymers

oxygen atoms density, particle size, and material's texture are important for the NF reaction mechanism [60]. Highly porous supports such as γ-alumina can ensure good dispersion of metal oxides and enhanced catalytic activity in gas reforming processes [61]. Moreover, the oxide of transition metals such as Co, Ni, Mo, W, and Ag supported on alumina have stimulated much research interest due to their activity in several processes, including selective oxidization of the NO_x [60, 62, 63].

According to the aforementioned research topics, in this study, the main objective is to obtain an in-depth understanding of catalyst-assisted NF process in the post-discharge of a low pressure (266 Pa) microwave plasma (MWP) fed with N_2 and O_2 gases. Within this study, alumina alone and supported metal oxide catalysts were prepared, characterized and their performances for NF were examined. To this end, Fourier Transform Infrared (FTIR) spectrometry was applied to measure products concentration. The effects of different parameters, namely calcination temperature (T_{cal}) and catalyst composition, were evaluated to reach optimal conditions within each parameter. The influences of catalyst properties on the chemical pathway of NF, as well as yield and efficiency, were observed and optimized.

2 Materials and Methods

2.1 Catalyst Preparation

Supported metal oxide catalysts were prepared by the conventional wet impregnation method reported on ref. [60]. Aqueous solutions of each metal oxide precursor were prepared separately by dissolving the corresponding precursor salts (ammonium heptamolybdate tetrahydrate, cobalt(II) nitrate hexahydrate, nickel nitrate hexahydrate-Merck 99.0%, and ammonium metatungstate hydrate-Alfa Aeser 99.0%) in distilled water in addition to 3:1 molar ratio of oxalic acid (Merck 99.5%) to ensure full dissolution of the precursor. Then, cylindrical pellets of highly porous γ-Al_2O_3 (Alfa Aeser, SA: 220 to 280 $m^2\ g^{-1}$) were added to the aqueous solutions and left for a few hours to ensure impregnation of γ-alumina. Finally, the solvent was mostly evaporated in a drying oven at 40°C first, at atmospheric pressure and later at reduced pressure. The dried solids were further heated at 110°C for 4 h and calcined under ambient atmosphere at 600°C for 4 h in a furnace. In this article, supported metal oxide catalysts are referred to as Al-M X, whereas Al refers to Al_2O_3, M indicating metal nature, and X shows metal loading relative to the weight of the catalyst.

2.2 Catalyst Characterization

Surface areas of the samples were measured via a Micromeritics ASAP 2020 system at 77 K, using the N_2 adsorption/desorption isotherms multipoint Brunauer-Emmett-Teller (BET) analysis method. The metal loading was controlled by the inductively coupled plasma optical emission spectroscopy (ICP-OES) using a VISTA-MAX VARIAN CCD Simultaneously ICP-OES spectrometer. The characterization of the crystalline structure of the catalyst after crushing into powder was obtained by XRD in a Bruker D8 Advanced X-ray diffractometer (40 kV, 40 mA) using a Cu-Kα (0.154 nm) radiation at a scanning rate of 0.2° s^{-1} from 10° to 100°. The nano-scale morphology of the catalyst samples was obtained by transmission electron microscopy (TEM-Philips CM 200). Further, selected area electron diffraction (SAED) was used to investigate the crystalline structure of the catalyst.

2.3 Experimental Setup

Figure 1 gives a schematic representation of the experimental setup utilized in this study. The microwave (2.45 GHz) generator is connected to the reactor via a surfaguide, and plasma is maintained in a quartz tube with a 14 mm inner diameter and 31 cm long. A pulse generator was used to operate the microwave in a pulse mode (pulse frequency = 0.5 kHz with 50% duty cycle). The base pressure of the setup, defined as the pressure reached under full operational capacity of the vacuum system in the absence of any gas inlet, was approximately 80 Pa. During the experiments, the working pressure, determined by the applied gas flow rate of 0.8 SLM, was about 266 Pa. Table 1 gives the specific experimental conditions investigated in this work. The discharge ignition takes place at the center of the quartz tube, where the waveguide is launched. A cylindrical vessel (with a volume of ≈6.2 cm^3) containing the catalysts (≈4 g) is in the post-discharge region, roughly 20 cm away from the discharge center. More information about this reactor and its specifications can be found elsewhere [64, 65].

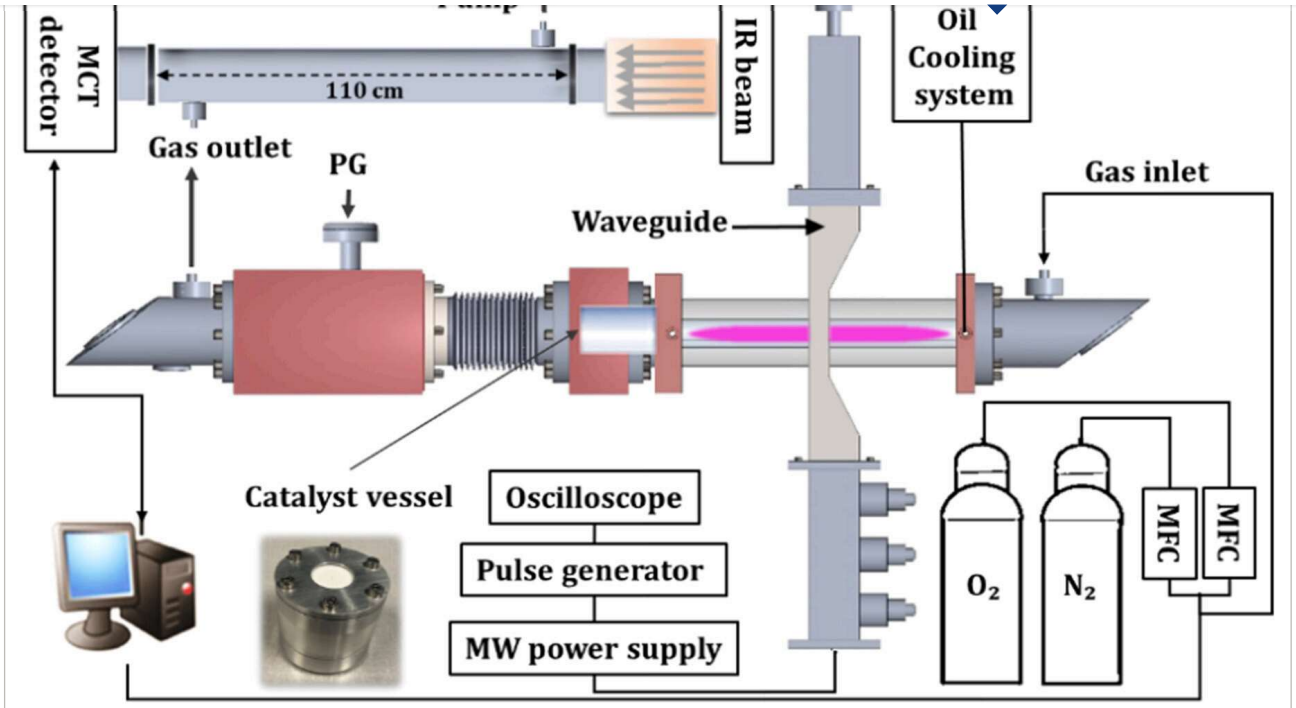

Figure 1

Open in figure viewer | PowerPoint

Schematic of the experimental setup.

Table 1. Specific conditions for MWP setup.

MW parameter	Value
Mean power	0.7 (kW)
Pulse frequency	0.5 (kHz)
Duty cycle	50%
Base pressure	80 (Pa)
Working pressure	266 (Pa)

constant operating conditions over a period of 100 min. After an initial transient, no significant variation in NO_x concentrations was observed, confirming that steady-state conditions were reached and maintained. Minor fluctuations in NO_x levels were attributed to the progressive removal of adsorbed water molecules, which frees surface vacancies and slightly favors NO_2 formation. All catalytic performances discussed in this work were evaluated under these steady-state conditions. The statistical error of NO_x concentration measurements is estimated to be about 5%–10% by repeating the measurements in the same experimental conditions.

Table 2. Specific parameters for FTIR spectrometer.

FTIR parameter	Specification
IR source	Mid–IR silicon carbide
Beam splitter	KBr (8000–350 [cm^{-1}])
Detector	MCT Mid band (ZnSe)
IR beam diameter	5–40 (mm)
Resolution	0.08 (cm^{-1})
Evaluating	Absorption
Optical path length	110 (cm)

3 Results and Discussion

3.1 Reaction Channels in the N_2-O_2 Catalyst-Assisted MWP

As mentioned before, MWP is highly effective in inducing vibrational excitation, making it a promising method for the NF process. Combining MWP with a catalyst either through an in-plasma catalyst (IPC) or a post-plasma catalyst (PPC) system, can significantly enhance the overall process. The IPC approach enables short-lived reactive species such as radicals, ions, photons, and electronically or vibrationally excited species to directly interact with the catalyst, offering additional pathways for targeted chemical conversions. However, in warm plasmas like microwave or gliding arc discharges, which typically operate at several thousand degrees Celsius, directly inserting the catalyst into the plasma zone is technically challenging. In such cases, the PPC configuration is more suitable, as it relies on long-lived reactive species (e.g., atomic and metastable species) that can escape the plasma and subsequently interact with the catalyst. Moreover, placing the catalyst in the post-discharge region allows for the separate evaluation of plasma and catalytic effects, due to the minimal direct interaction between the plasma and the catalyst. In Figure 2, the FTIR absorption spectra of MWP alone and with γ-Al_2O_3 catalyst are depicted. The absorption bands of NO_2 and NO were recorded in spectral intervals of 1580–1650 cm^{-1} and 1770–1960 cm^{-1} and can be assigned to the fundamental vibrational transitions in the ground electronic states of NO_2 and NO, respectively [66-68]. The absorption bands corresponding to the NO_x molecules are given in Table 3. Indeed, MWP with a N_2:O_2 (1:1) gas mixture ratio was selected based on preliminary optimization experiments, induce only a double branch NO infrared transitions of $X^2\Pi(v=1) \leftarrow X^2\Pi(v=0)$ with a band head at 1876.2 cm^{-1} [66, 67]. These transitions are also in good agreement with the HITRAN database [69]. Introducing γ-Al_2O_3 into the system results in NO_2 molecule synthesis, which has fundamental infrared transitions of $X^2A_1(v=001) \leftarrow X^2A_1(v=000)$ with the band head at 1616.9 cm^{-1} [68].

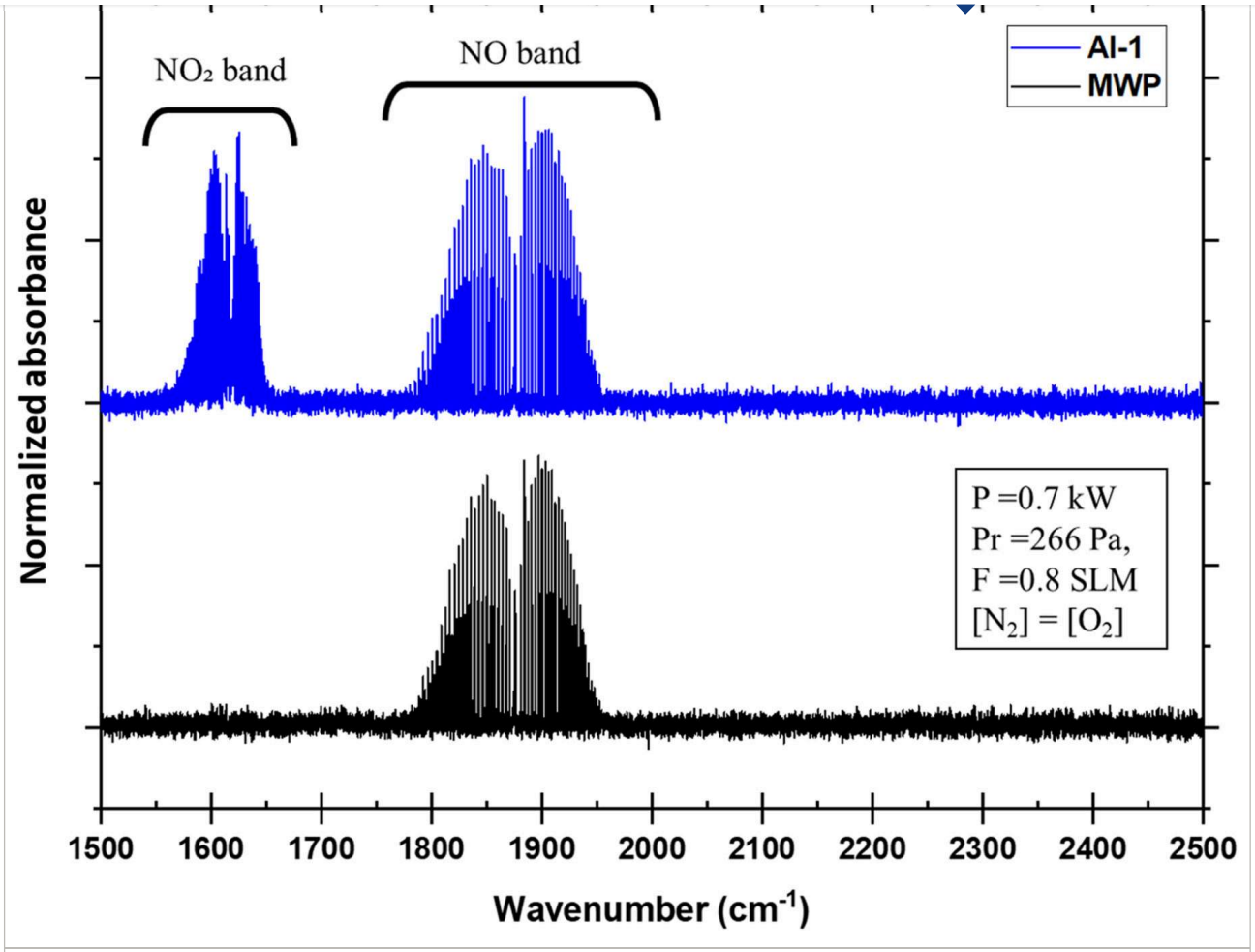

Figure 2

Open in figure viewer | PowerPoint

FTIR spectra with y-axis offset of microwave plasma (MWP) in black, and MWP with γ-Al_2O_3 catalyst (Al-1) in blue.

Table 3. Assignments of the absorption bands monitored by FTIR.

position. As far as we know, the synthesis mechanism of NO_2 in the post-discharge zone in the presence of a catalyst has not been studied yet, although several articles have explained the formation of NO_2 in the IPC system [46]. Hence, to expand our knowledge about existing emission lines of reactive species OES was used. A typical broad emission spectrum from the discharge active zone for N_2-O_2 gas mixtures is shown in Figure 3. Table 4 provides a list of the most radiative species generated in the MW plasma zone which are involved in the NO_x synthesis process. Generally, due to the highly endothermic nature of N_2 dissociation, elevated temperature is necessary [72]. In thermal processes, the direct dissociation of both N_2 and O_2 molecules is essential, but this requires approximately 15 eV to overcome their activation energy barriers. In contrast, in NTPs, NO_x formation from N_2-O_2 mixture is initiated through electron impacts [29]. In this way, energetic electrons driven by plasma introduce various vibrational excitations of N_2 and O_2, resulting in the dissociation and generation of N and O atoms.

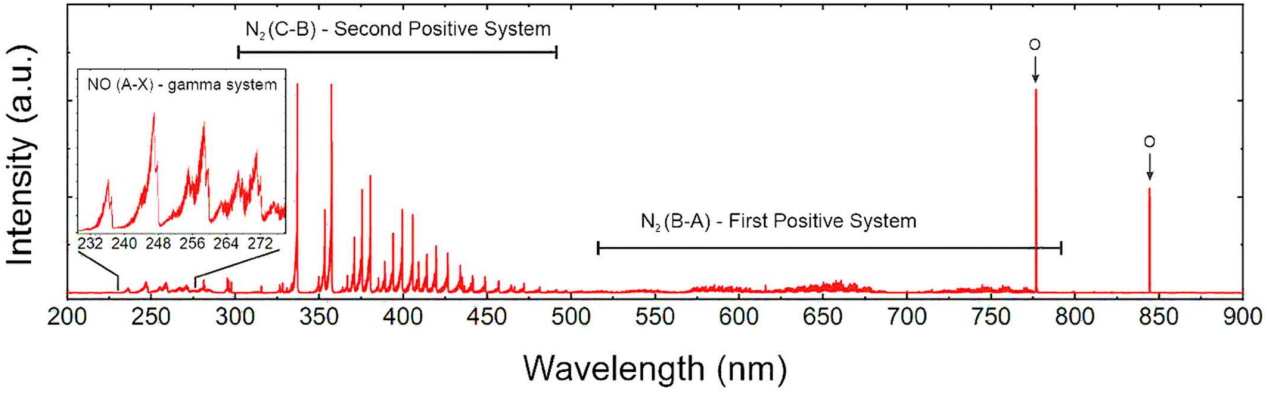

Figure 3

Open in figure viewer | PowerPoint

Axial emission spectrum in the pulsed MW discharge for N_2:O_2 (1:1) gas mixtures at an average applied power of 0.7 kW and a gas pressure of 266 Pa.

Table 4. Assignments of the emission bands monitored by OES.

Species	Wavelengths covered (nm)	Transitions	System	Reference
NO	205–275	$A^2\Sigma^+ \rightarrow X^2\Pi$	γ system	
N_2	275–500	$C^3\Pi_u \rightarrow B^3\Pi_g$	2nd positive	
N_2	520–780	$B^3\Pi_g \rightarrow A^3\Sigma_g$	1st positive	[70, 71]
O	777.3	$O(3p^5P \rightarrow 3s^5S)$	—	
O	844.6	$O(3p^3P \rightarrow 3s^3S)$	—	

Initially, the vibrational excitation mechanism of N_2 reduces the bond strength of the molecule and allows for vibrational dissociation of N_2 for NO generation in non-thermal conditions through reactions with atomic oxygen (R.1). In this reaction, $O(^3P)$ denotes ground-state atomic oxygen, whose effective lifetime in the low-pressure reactor is governed primarily by heterogeneous wall recombination and is typically on the order of 10^{-2}–10^{-1} s. Additional NO generation can also be achieved by a secondary exothermic process through

O_2, N_2-N and N_2-O collisions. The influence of these V-T channels becomes progressively smaller with the increase of (R. 1) reaction rate, which is the predominant mechanism for the formation of NO and N [30]. The formation of NO at different states such as NO(X) and NO(A) from the NO γ-system (where X and A stand for the ground and excited states, respectively) was investigated by Loureiro et al. [31] via modeling in the pressure range of 13-1330 Pa. They showed that NO(X) state formation mainly takes place via the reaction (R.1), and destruction of NO(X) occurs via reverse Zeldovich mechanisms (R.2). Oppositely, NO(A) is predominantly produced by collisions of metastable N_2(A) with ground state NO(X) molecules. This NO(A) is lost by quenching with N_2, O_2 and NO [74]. Apart from NO formation through N_2 vibrational states (R.1), NO can be formed as well through other pathways likely through electronically excited N_2, namely $N_2(B^3\Pi_g)$, upon reaction with O atoms or/and due to the reaction of N atoms with O_2 (R.2). On the other hand, a significant NO loss process results from the recombination of NO with O atoms leading to NO_2 formation through reaction (R.3). In general, we conclude that the N_2 vibrational pathway is important for NO formation, in the conditions under study. Typically, in the MW plasmas, the gas discharge temperature is in the range of 1000°C to 4000°C [29]. In such elevated temperatures, NO molecules are more stable than NO_2 molecules whereas NO_2 can be dissociated into the reactants in the reverse reactions (R.3 and R.4). Bahnamiri et al. studied the influence of gas temperature on NO and NO_2 formation in the MWP system [71]. According to the authors, NO also is the final product as NO_2 cannot be detected due to its instability inside the reactive zone of plasma. In presence of catalyst in the post-discharge zone, the formation of NO_2 is initiated over the catalyst where the temperature drops to about 300°C. In this condition, the reactive species, whether generated by plasma or regenerated due to recombination reactions, can partially reach the catalyst surface to form NO_x species. Formation of NO_2 is more probable on alumina catalyst through stepwise reactions (R.5 and R.6) of adsorbed atomic oxygen with gaseous NO molecule to give away NO_2 molecule (Eley-Rideal Model [56]).

(R.5)

(R.6)

This reaction pathway has been reported to dominate NO_2 formation in DBD plasma–catalytic systems operating in an IPC configuration [46]. In such systems, plasma-generated species, including atomic oxygen $O(^3P)$, can reach the catalyst surface with limited transport losses and may therefore contribute significantly to surface reactions.

In contrast, in the present PPC configuration, the direct involvement of short-lived electronically excited oxygen species originating from the plasma phase is unlikely. The relatively long distance between the plasma active zone and the catalyst (approximately 20 cm, corresponding to a gas residence time of about 2 ms at a gas velocity of 100 m s^{-1}) strongly limits the survival of such excited species due to collisional quenching and relaxation processes. Consequently, we assume that NO_2 formation over the catalyst is primarily driven by long-lived species, in particular ground-state atomic oxygen $O(^3P)$, as well as by species generated through recombination reactions and NO decomposition (R1) occurring in the vicinity of the catalyst surface.

3.2 Catalytic Activity of Al_2O_3 Prepared With Various T_{cal}

The γ-Al_2O_3 derived from the boehmite precursor is the most important alumina for industrial catalytic applications. However, other alumina phases exhibit several metastable phases, so-called “transition alumina phases”, such as δ, θ, η, κ, and thermodynamically stable α phase also playing a critical role in catalytic applications. Being highly relevant in catalytic applications, in the past, the research on transition alumina was motivated by the interest in understanding the nature of surface properties, and their adsorptive and catalytic behavior. Different structures of alumina can provide a diversity of surface-active sites for catalytic activity. In this work, to investigate the impact of different structures of alumina, γ-Al_2O_3 was calcined at different temperatures and was then studied regarding NO_x production (Figure 4). From this figure, we can observe that the T_{cal} does not significantly impact the NO production, supporting the fact that, in our experimental conditions, the NO production is not significantly depending on the catalytic activity of alumina which is consistent with a NO production dominated by plasma phase reactions. On the other hand, it appears that the T_{cal} significantly impacts the NO_2 formation since we observe a dependence of the NO_2 density as a function of the T_{cal}. Among the samples, Al_2O_3 calcined at 800°C shows a slightly better performance than the others. To correlate their properties to NO_x formation behavior, more detailed studies about the alumina structures and properties were performed.

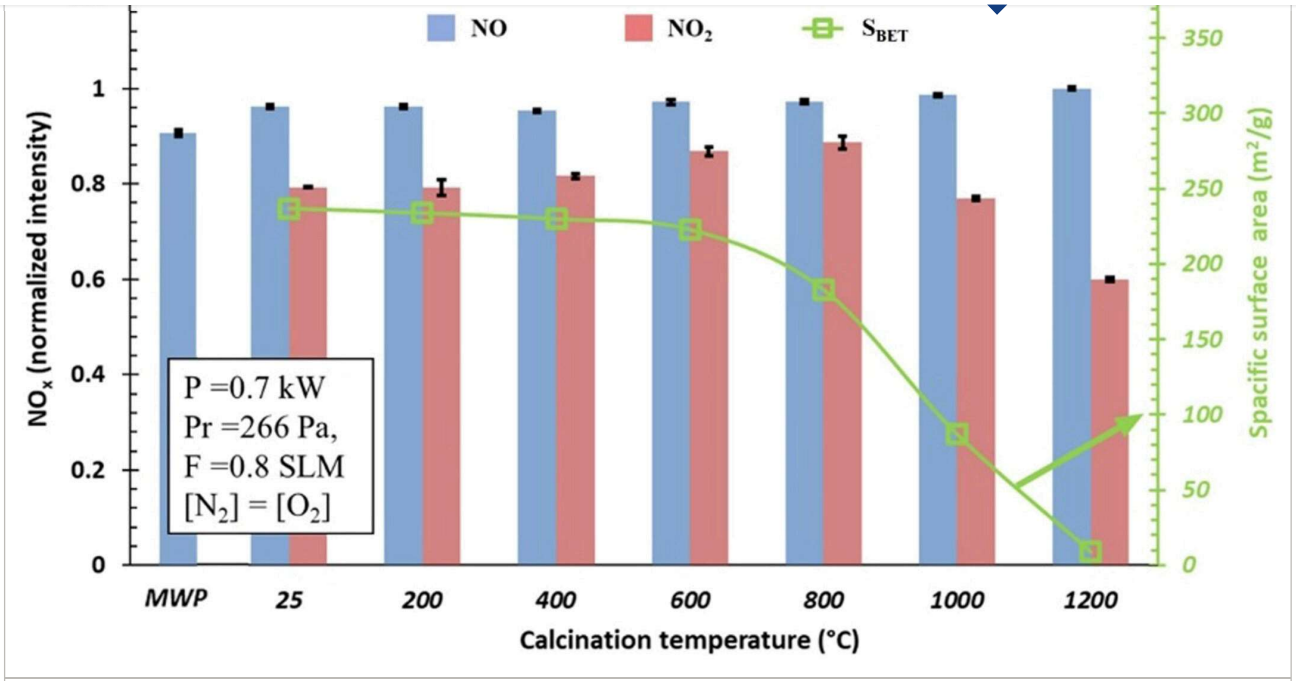

Figure 4

Open in figure viewer | PowerPoint

NO_x formation depending upon the different T_{cal} of alumina used as catalyst in NF by MWP. The specific surface area of catalysts (S_{BET}) is represented by the green line.

3.3 Evaluation of Catalyst Features

The results of the surface area, pore size and volume for Al_2O_3 after calcination at different temperatures are shown in Figure 5. Despite a drop in surface area from 240 to 10 $m^2\ g^{-1}$ (25°C–1200°C), NO production remains nearly unchanged (Figure 4), indicating it is not surface area-dependent. NO_2 formation correlates with the S_{BET} of the catalysts, with the alumina calcined at 800°C showing the highest NO_2 output among all T_{cal} variants. At first look, it seems counterintuitive, as it has a reduced BET surface area and pore volume compared to the others. The observed phenomenon can be rationalized by the minimal alteration in surface texture detected during thermal treatment, as evidenced by the absence of significant changes in catalyst pore size (refer to Figure 5). The reduction in the BET surface area is likely attributable to the process of particle sintering and agglomeration during thermal treatment of catalysts. Hence, in this scenario, the predominant NO_2 production cannot be ascribed to the porosity characteristics, despite their recognized impact on influencing catalyst activities. As proven in literature, alumina at different temperatures provides different structures that could explain dissimilar catalytic behaviors.

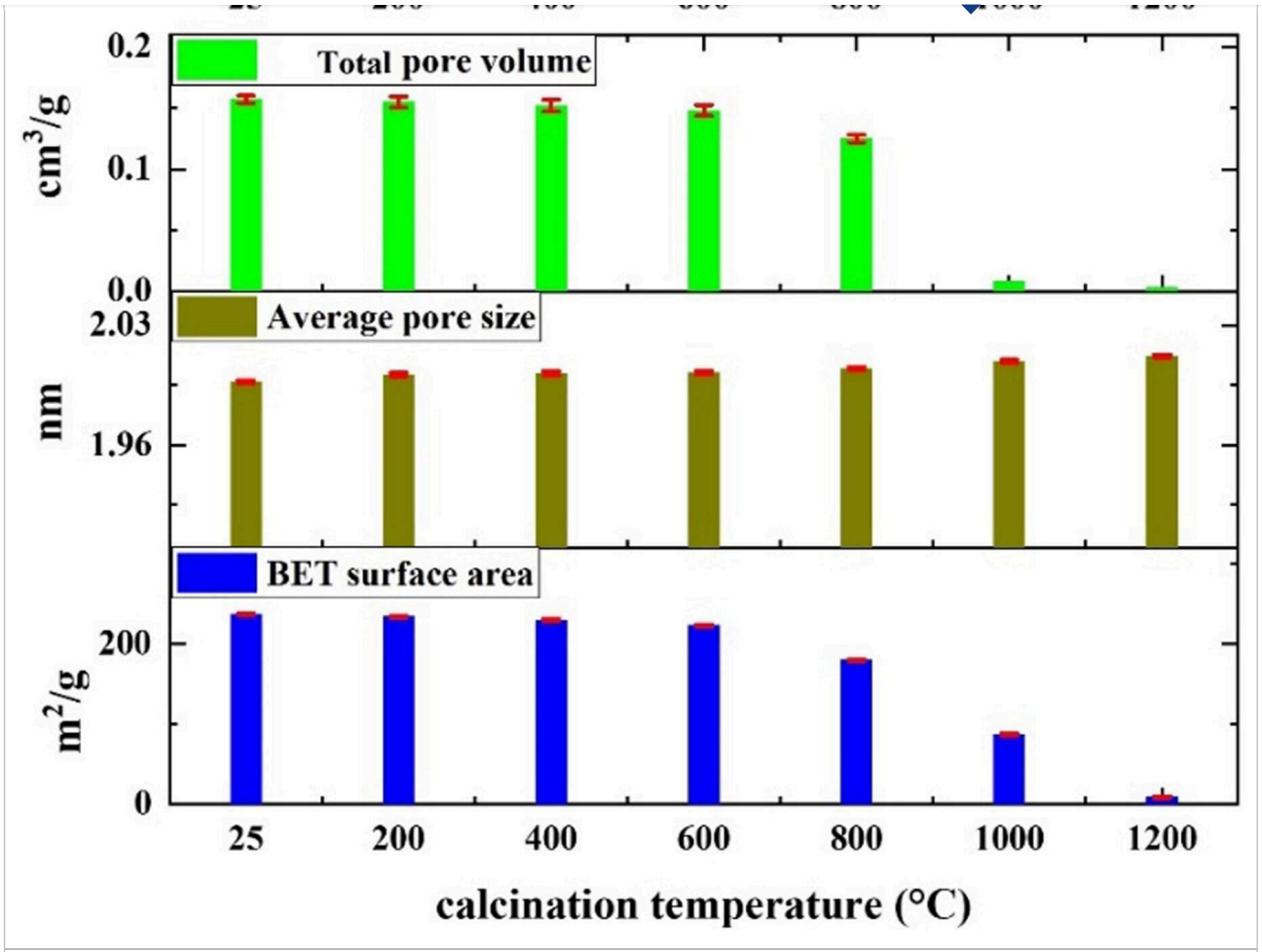

Figure 5

Open in figure viewer | PowerPoint

Effect of different T_{cal} of alumina on the porosity characteristics of the catalyst.

3.4 Study of Catalyst Phase Structure

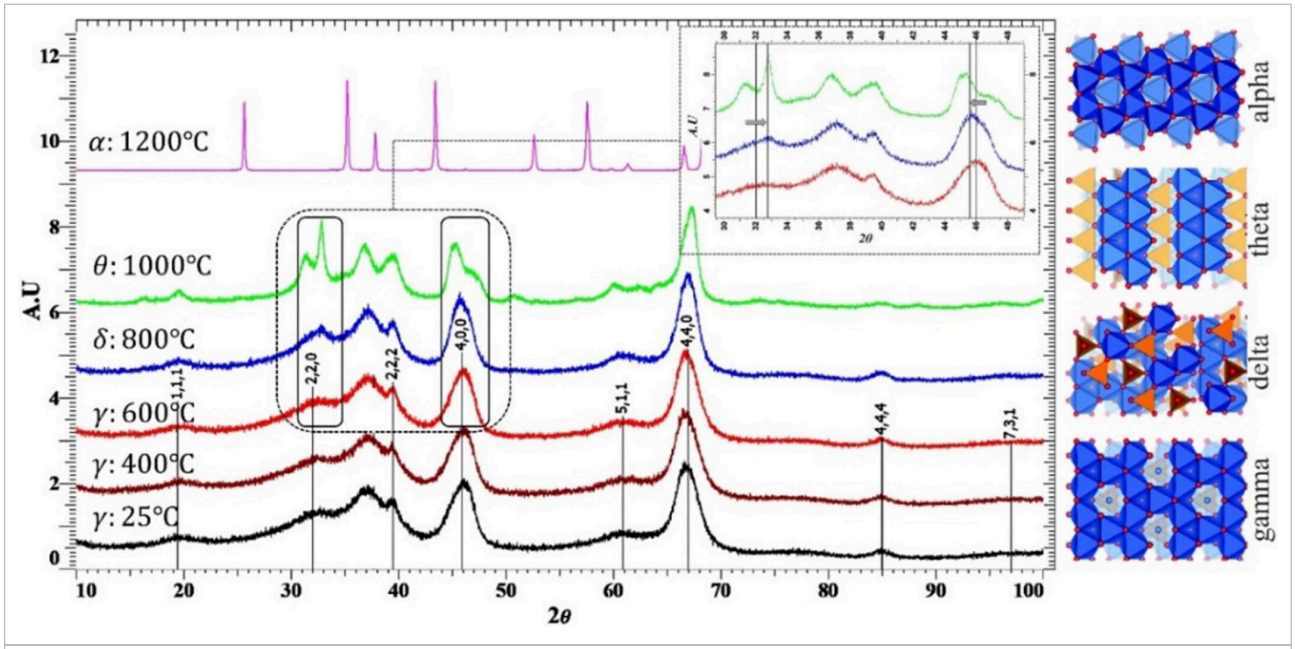

Figure 6

Open in figure viewer | PowerPoint

X-ray diffractogram of the alumina at different T_{cal} (from 25°C at the bottom increasing to 1200°C on the top) showing phase change of alumina and beside the crystal structures of each phase were indicated (red dot: O atoms; blue dot: Al atoms; blue and yellow polygons: octahedral and tetrahedral structures, respectively).

In XRD patterns, the δ-Al_2O_3 formation is often recognized by gradual shifting, splitting of diffraction peaks, as well as by broadening of characteristic shoulders (see black blocks and zoomed area in Figure 6). The diffraction features can be very subtle and readily masked by γ-Al_2O_3, which may be one of the reasons why it has sometimes been neglected in the analysis. Nevertheless, during the phase transformation of γ-Al_2O_3, the δ phase shows better results in NO_2 production, which may be due to the reformation of the alumina microstructure into the δ phase. It is conventionally explained in terms of the gradual reordering from γ to δ-alumina starting at 800°C and ending at 900°C. At 800°C, the phase transformation is in its early stages and the δ phase is not fully completed. However, δ alumina at 800°C does not show any distinguishable characteristic peaks in the XRD pattern, which contains a proportion of both tetrahedral and octahedral structure (≈ 0.6). In general, it is believed that during this transformation, different distortions and defects than γ-Al_2O_3 are introduced into the crystal structure to form new surface sites, which may be the main reason for NO_2 enhancement [78]. In addition, this transition phase has different oxygen sub-lattices in a face-centered cubic crystal (fcc) structure. In transition phases, with the fcc crystal arrangement, oxygen anions and aluminum cations appear in many proportions with octahedral and tetrahedral structures [79]. But, correlating NO_2 increment with this transition phase is a challenging task due to the coexistence of distinct phases with similar structures and distorted crystal lattices. Phase transformation sequence from metastable alumina structures toward the stable α phase during heating is presented by H. Dexert et. al. [77] The structural change from the δ phase into θ (with the 50% ratio of both octahedral and tetrahedral Al) and α (100% of octahedral Al) phases with its close-packed crystal (hcp) structure agrees with a sharp decrease of S_{BET} as observed in Figure 5 that also corresponds to low activity of catalysts regarding NO_2 production.

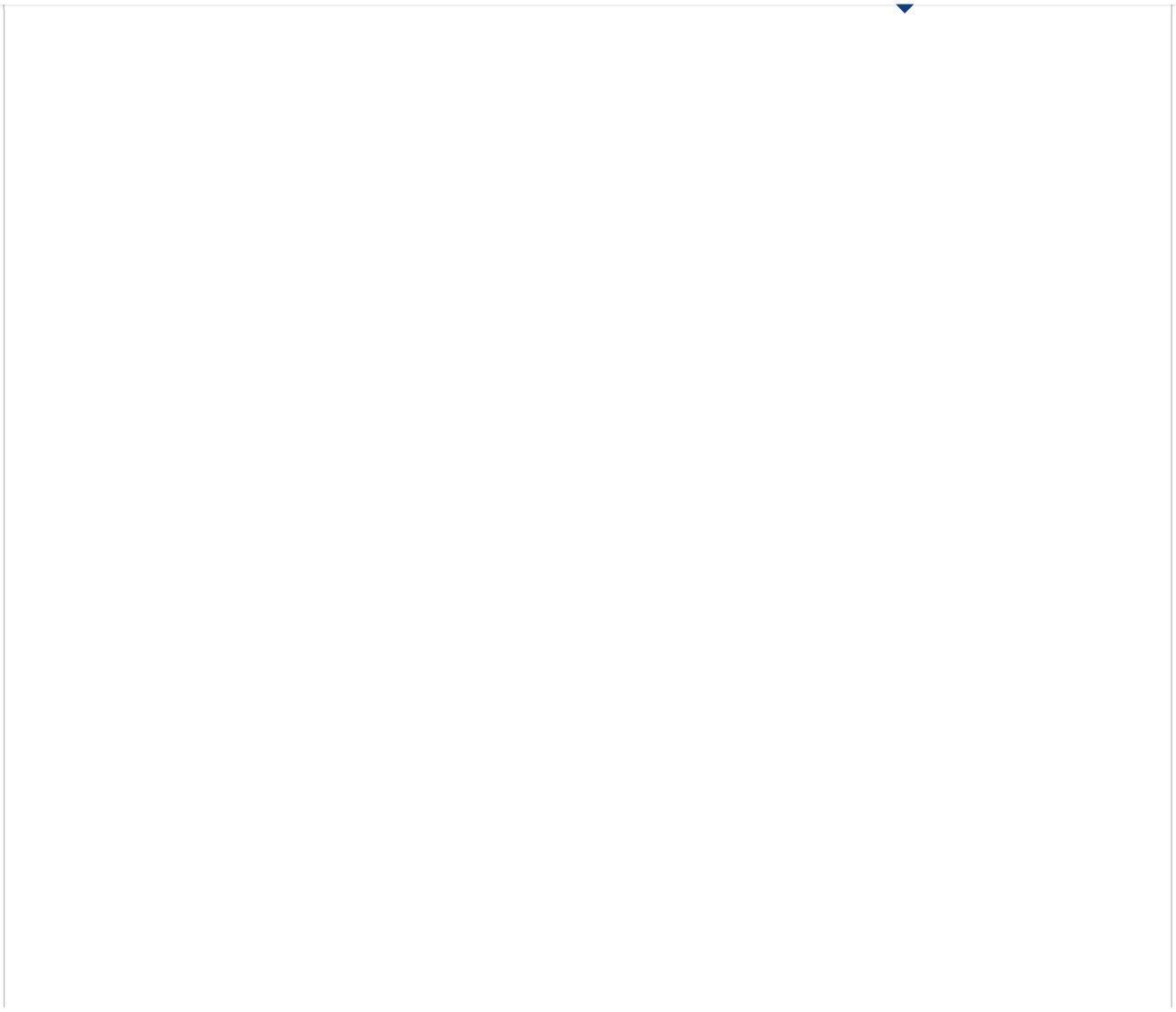

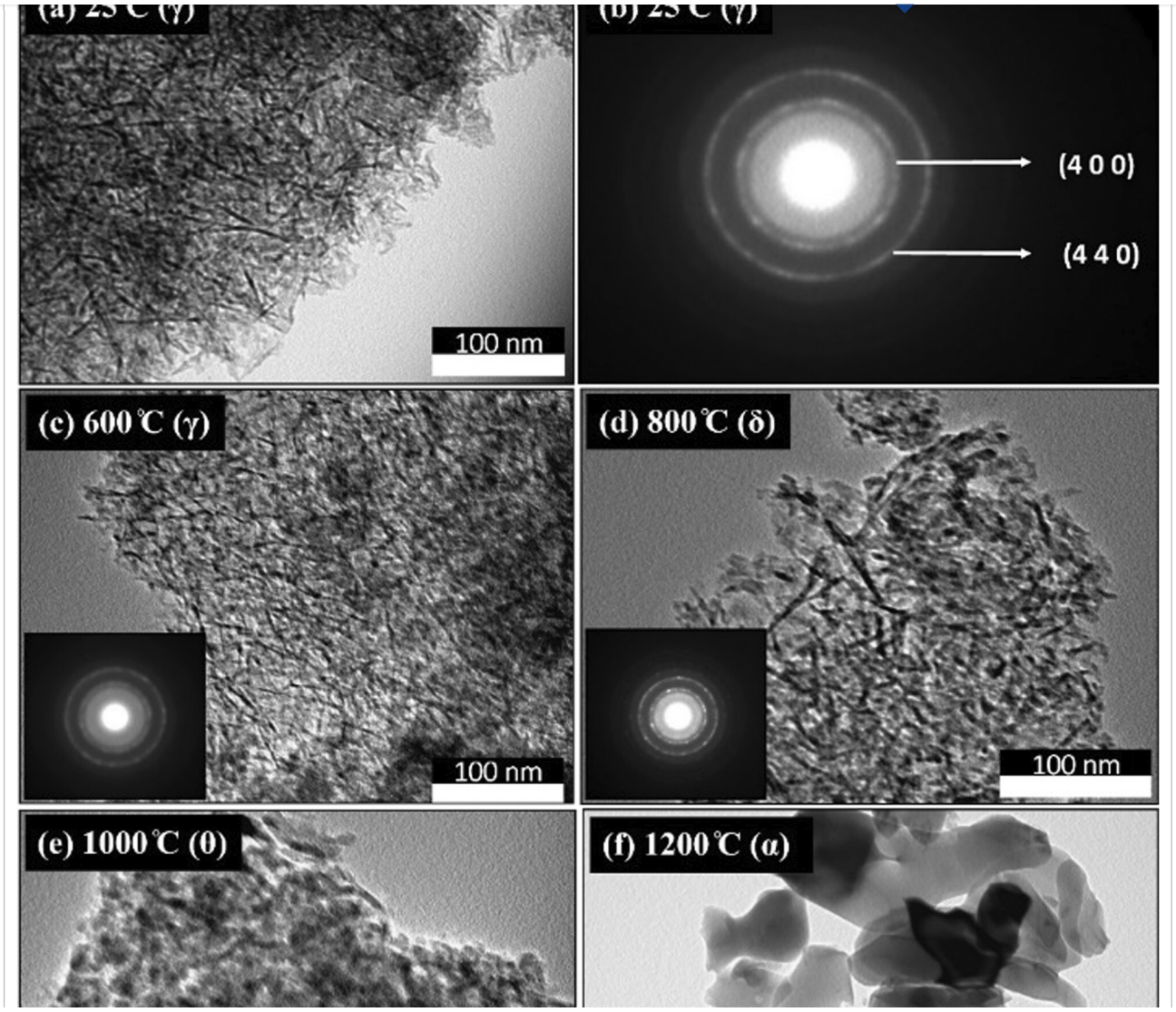

Figure 7

Open in figure viewer | PowerPoint

TEM micrographs and SAED patterns (inset graphs) of the alumina at different T_{cal}: (a) 25°C, (b) 25°C, (c) 600°C, (d) 800°C, (e) 1000°C, and f) 1200°C.

3.6 Effect of Catalyst Composition

In the context of the N_2 activation in catalyst-assisted plasma, a common strategy involves enhancing the back donation of ᴅ-electrons from transition metal oxides into the π antibonding orbital of N_2 [80, 81]. In literature, among the few studies on the topic, the best results were achieved with MoO_3 deposited on the inner wall of a RF plasma reactor [37, 57]. And yet, alumina is widely used as a catalyst support due to its high surface area, porosity, and thermal and mechanical stability, among other support materials reported in the literature [82-84]. Therefore, we aimed to enhance the NF process in the post-discharge zone of MWP by applying Mo oxide impregnated on distinct phases of the Al_2O_3 as a support catalyst. Figure 8 shows the normalized NO_x concentration measured for the MWP discharge alone and alumina supported with a 5 wt% Mo oxide loaded at different T_{cal}. For all catalysts, we observed a slight enhancement of NO and NO_2 signals' intensity compared to the plasma process (MWP) alone and a slight positive effect on NO_x production due to the presence of Mo, particularly for calcination at 600°C and 800°C (γ and δ phases). Literature suggests many chemical reaction pathways for NO_x formation in NTPs through catalytic routes (e.g., with ionized species or atomic nitrogen, etc.). Nevertheless, Gicquel et al. [57] proposed the following reaction mechanism for NO_x synthesis on MoO_3 catalysts:

(R.7)

(R.8)

(R.9)

(R,10)

(R.11)

(R.12)

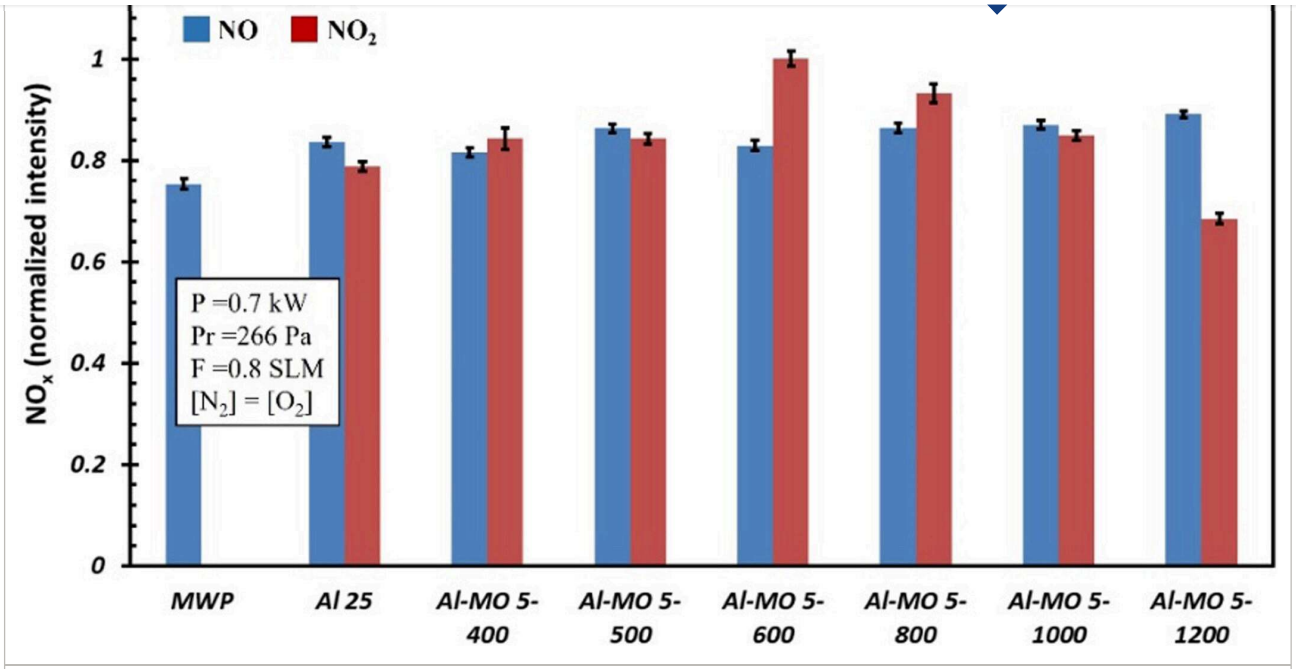

Figure 8

Open in figure viewer | PowerPoint

NO_x formation depending upon the different T_{cal} of alumina with 5 wt% Mo oxide loading used in MWP.

The above-mentioned reactions were predominant in an IPC system, in which MoO_3 was deposited on the inner wall of a RF plasma reactor. In this context, N_2* denotes vibrationally excited nitrogen molecules, $N_2(X, v \gg 0)$, and possibly metastable $N_2(A^3\Sigma_u^+)$, rather than short-lived electronically excited states. Based on the reactive species identified in the MWP system by OES (Table 4), a similar NO_x formation pathway (R. 7–R. 12) is likely operative in the present experiments. It should be noted that OES detects only radiative excited states and therefore does not directly represent ground-state or metastable species. Nevertheless, consistent with observations of the catalytic activity of alumina at the PPC position, the limited performance of Mo-based catalysts in the PPC configuration is more plausibly attributed to catalyst-specific surface phenomena-such as adsorption efficiency and surface reaction pathways-rather than to the intrinsic lifetimes of plasma-generated species. Comparable behavior has been reported for air plasma jet systems coupled with heterogeneous catalysis [85].

To understand the performance of catalysts regarding NO_x formation and to clarify their structure, XRD data were collected (Figure 9). For samples with T_{cal} below 600°C the expected XRD lines of γ-Al_2O_3 were observed. The small boost in NO_x with γ phase catalysts seems to be due to the gradual formation of MoO_3 monolayer systems, as often referred to in literature. Spreading of MoO_3 species over the support surface can introduce new active sites [86-88]. In this way, a layer of MoO_3 on the support can modify the surface free energy of the system with less impact on the bulk structure, as there is no evidence of Mo crystallite peaks or other peaks deformation on the XRD pattern of the sample calcined at 600°C. Mo-related peaks only appear in Mo-loaded samples with T_{cal} above 800°C with peaks at 2θ of 15.6, 20.9°, 22.2°, 23.2°, and 23.5° corresponding to $Al_2(MoO_4)_3$ structure [89]. In literature, it is mentioned that apart from the preparation method, due to the high dispersion ability of Mo on the alumina support at higher thermal treatment temperature (> 600°C), $Al_2(MoO_4)_3$

catalyst (Al-Mo 5 or Al-W 5), a 30% enhancement in NO_x production is observed. Of this enhancement, 25% can be attributed to the contribution of γ-Al_2O_3, accounting for approximately 10% of NO and 15% of NO_2 formation.

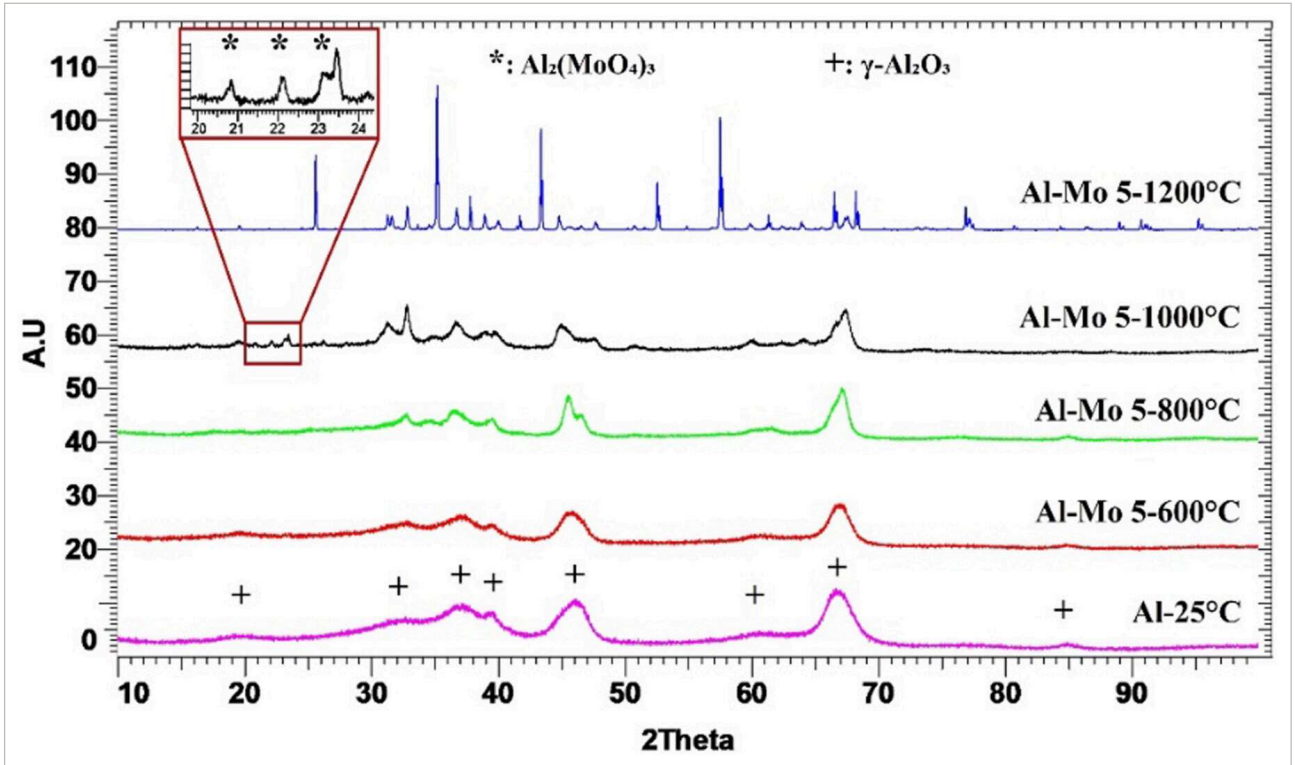

Figure 9

Open in figure viewer | PowerPoint

XRD patterns of Mo oxide loading (5 wt%) on different Al_2O_3 phases (red block indicates peaks of $Al_2(MoO_4)_3$ formation).

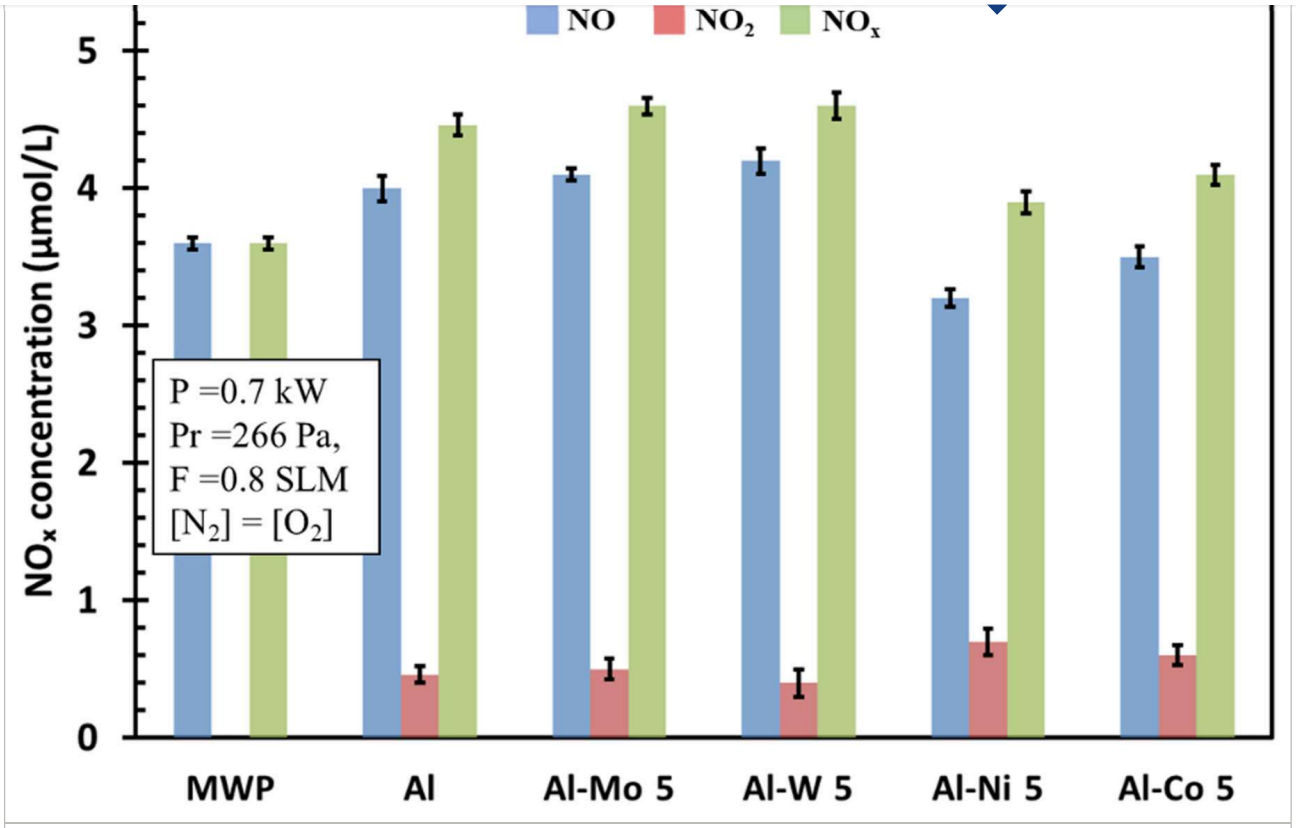

Figure 10

Open in figure viewer | PowerPoint

Effect of different metal oxides loading (5 wt%) on γ-Al_2O_3 in NO_x production.

4 Conclusions

Nitrogen fixation via catalyst-assisted, low-pressure pulsed microwave plasma was investigated using alumina-based heterogeneous catalysts. The catalysts were placed in the post-discharge zone of an MWP fed with an N_2–O_2 gas mixture, and their performance toward NO_x formation was evaluated by FTIR spectroscopy. In contrast to plasma operation without a catalyst, the presence of alumina enabled the formation of NO_2, demonstrating that alumina provides an additional reaction pathway at the gas–solid interface and acts as an active catalyst for nitrogen fixation.

Thermal treatment of alumina revealed a limited influence of calcination temperature on NO formation (~ 10%), whereas a clear correlation with NO_2 production (~ 15%) was

compared to plasma alone was achieved, with about 25% attributed to γ-Al_2O_3. The highest NO_x yield (~4.5%) was obtained with the lowest energy cost (~15 MJ mol^{-1}), corresponding to a maximum energy efficiency of ~0.6% for the Al–Mo 5 catalyst.

Acknowledgments

The research is supported by the excellence of science FNRS-FWO program, "NITROPLASM" project, EOS ID: O005118F.

Conflicts of Interest

The authors declare that they have no known competing interests or personal relationships that could have appeared to influence the work reported in this article.

Data Availability Statement

The data that support the findings of this study are available from the corresponding author upon reasonable request.

References

1 M. O. Mclinden and M. L. Huber, "(R)Evolution of Refrigerants," *Journal of Chemical and Engineering Data* **65** (2020): 4176–4193, https://doi.org/10.1021/acs.jced.0c00338.

CAS | Web of Science® | Google Scholar

2 M. Shomali, D. Opie, T. Avasthi, and A. Trilling, "Nitrogen Dioxide Sterilization in Low-Resource Environments: A Feasibility Study," *PLoS One* **10** (2015): e0130043, https://doi.org/10.1371/-JOURNAL.PONE.0130043.

PubMed | Web of Science® | Google Scholar

3 R. Muto and N. Hayashi, "Sterilization Characteristics of Narrow Tubing by Nitrogen Oxides Generated in Atmospheric Pressure Air Plasma," *Scientific Reports* **13** (2023): 6947, https://doi.org/10.1038/s41598-023-34243-3.

CAS | PubMed | Web of Science® | Google Scholar

4 M. Culture, *Ignition! an Informal History of Liquid Rocket Propellants* (Rutgers University Press, 1972).

Google Scholar

5 H. A. Sorgenti and G. F. Sachsel, "Nitric Acid Manufacture—Theory and Practice," *Industrial and Engineering Chemistry* **52** (2002): 101–104, https://doi.org/10.1021/IE50602A019.

Google Scholar

6 R. Kumar, S. Saha, S. Dhaka, et al., "Remediation of Cyanide-Contaminated Environments Through Microbes and Plants: A Review of Current Knowledge and Future Perspectives," *Geosystem Engineering* **20** (2017): 28–40, https://doi.org/10.1080/12269328.2016.1218303.

CAS | Web of Science® | Google Scholar

9 L. Rosa and P. Gabrielli, "Energy and Food Security Implications of Transitioning Synthetic Nitrogen Fertilizers to Net-Zero Emissions," *Environmental Research Letters* **18** (2023): 014008, https://doi.org/10.1088/1748-9326/aca815.

CAS | Web of Science® | Google Scholar

10 M. Appl: The Haber-Bosch Heritage: The ammonia production technology. In 50th Anniversary of the IFA Technical Conference. Seville Spain (1997).

Google Scholar

11 V. Smil, *Enriching the Earth: Fritz Haber, Carl Bosch, and the Transformation of World Food Production* (MIT press, 2004).

Google Scholar

12 A. S. Travis, " Electric Arcs, Cyanamide, Carl Bosch and Fritz Haber." *The Synthetic Nitrogen Industry in World War I: Its Emergence and Expansion* (Springer, 2015), 17–72, https://doi.org/10.1007/978-3-319-19357-1_2.

Google Scholar

13 D. Li, L. Zan, S. Chen, et al., "Direct Conversion of N2 and O2: Status, Challenge and Perspective," *National Science Review* **9** (2022), https://doi.org/10.1093/nsr/nwac042.

Web of Science® | Google Scholar

14 K. H. R. Rouwenhorst, F. Jardali, A. Bogaerts, and L. Lefferts, "From the Birkeland-Eyde Process Towards Energy-Efficient Plasma-Based NO: Xsynthesis: A Techno-Economic Analysis," *Energy and Environmental Science* **14** (2021): 2520–2534, https://doi.org/10.1039/d0ee03763j.

CAS | PubMed | Google Scholar

15 S. Ghavam, M. Vahdati, I. A. G. Wilson, and P. Styring, "Sustainable Ammonia Production Processes," *Frontiers in Energy Research* **9** (2021), https://doi.org/10.3389/fenrg.2021.580808.

Web of Science® | Google Scholar

16 N. Cherkasov, A. O. Ibhadon, and P. Fitzpatrick, "A Review of the Existing and Alternative Methods for Greener Nitrogen Fixation," *Chemical Engineering and Processing: Process Intensification* **90** (2015): 24–33, https://doi.org/10.1016/J.CEP.2015.02.004.

CAS | Web of Science® | Google Scholar

17 H. Chen, D. Yuan, A. Wu, X. Lin, and X. Li, "Review of Low-Temperature Plasma Nitrogen Fixation Technology," *Waste Disposal and Sustainable Energy* **3** (2021): 201–217.

PubMed | Google Scholar

18 S. Li, J. Medrano, V. Hessel, and F. Gallucci, "Recent Progress of Plasma-Assisted Nitrogen Fixation Research: A Review," *Processes* **6** (2018): 248.

21 W. Wang, B. Patil, S. Heijkers, V. Hessel, and A. Bogaerts, "Nitrogen Fixation by Gliding Arc Plasma: Better Insight by Chemical Kinetics Modelling," *Chemsuschem* **10** (2017): 2145–2157, https://doi.org/10.1002/cssc.201700095.

CAS | PubMed | Web of Science® | Google Scholar

22 F. Jardali, S. Van Alphen, J. Creel, et al., "NOx Production in a Rotating Gliding Arc Plasma: Potential Avenue for Sustainable Nitrogen Fixation," *Green Chemistry* **23** (2021): 1748–1757, https://doi.org/10.1039/d0gc0352-1a.

CAS | Web of Science® | Google Scholar

23 S. Van Alphen, H. Ahmadi Eshtehardi, C. O'Modhrain, et al., "Effusion Nozzle for Energy-Efficient NOx Production in a Rotating Gliding Arc Plasma Reactor," *Chemical Engineering Journal* **443** (2022): 136529.

CAS | Web of Science® | Google Scholar

24 T. Kim, S. Song, J. Kim, and R. Iwasaki, "Formation of NOX From Air and N2/O2 Mixtures Using a Nonthermal Microwave Plasma System," *Japanese Journal of Applied Physics* **49** (2010), https://iopscience.iop.org/article/10.1143/JJAP.49.126201.

Web of Science® | Google Scholar

25 S. Kelly and A. Bogaerts, "Nitrogen Fixation in an Electrode-Free Microwave Plasma," *Joule* **5** (2021): 3006–3030, https://doi.org/10.1016/j.joule.2021.09.009.

CAS | Web of Science® | Google Scholar

26 B. S. Patil, J. Rovira Palau, V. Hessel, J. Lang, and Q. Wang, "Plasma Nitrogen Oxides Synthesis in a Milli-Scale Gliding Arc Reactor: Investigating the Electrical and Process Parameters," *Plasma Chemistry and Plasma Processing* **36** (2016): 241–257, https://doi.org/10.1007/-S11090-015-9671-4.

CAS | Web of Science® | Google Scholar

27 N. Britun, V. Gamaleev, and M. Hori, "Evidence of Near-The-Limit Energy Cost No Formation in Atmospheric Spark Discharge," *Plasma Sources Science and Technology* **30** (2021): 08LT02.

CAS | Web of Science® | Google Scholar

28 R. J. Wandell, H. Wang, R. K. M. Bulusu, R. O. Gallan, and B. R. Locke, "Formation of Nitrogen Oxides by Nanosecond Pulsed Plasma Discharges in Gas–Liquid Reactors," *Plasma Chemistry and Plasma Processing* **39** (2019): 643–666, https://doi.org/10.1007/S11090-019-09981-W.

CAS | Web of Science® | Google Scholar

29 A. A. Fridman, *Plasma Chemistry* (Cambridge University Press, 2008).

Google Scholar

32 R. I. Asisov, V. K. Givotov, V. D. Rusanov, and A. Fridman, "High Energy Chemistry (Khimia Vysokikh Energij)," *Soviet Physics* **14** (1980): 366.

Google Scholar

33 M. Heintze and B. Pietruszka, "Plasma Catalytic Conversion of Methane Into Syngas: The Combined Effect of Discharge Activation and Catalysis," *Catalysis Today* **89** (2004): 21–25.

CAS | Web of Science® | Google Scholar

34 J. Van Durme, J. Dewulf, C. Leys, and H. Van Langenhove, "Combining Non-Thermal Plasma With Heterogeneous Catalysis in Waste Gas Treatment: A Review," *Applied Catalysis, B: Environmental* **78** (2008): 324–333, https://doi.org/10.1016/J.APCATB.2007.09.035.

CAS | Web of Science® | Google Scholar

35 H. Long, S. Shang, X. Tao, Y. Yin, and X. Dai, "CO2 Reforming of CH4 by Combination of Cold Plasma Jet and Ni/γ-Al2O3 Catalyst," *International Journal of Hydrogen Energy* **33** (2008): 5510–5515.

CAS | Google Scholar

36 A. J. Zhang, A. M. Zhu, J. Guo, Y. Xu, and C. Shi, "Conversion of Greenhouse Gases into Syngas via Combined Effects of Discharge Activation and Catalysis," *Chemical Engineering Journal* **156**, no. 3 (2010): 601–606.

CAS | Web of Science® | Google Scholar

37 D. Rapakoulias, S. Cavadias, and J. Amouroux, "Processus Catalytiques Dans Un Réacteur À Plasma Hors D'Équilibre Ii. Fixation De L'azote Dans Le Système N2-O2," *Revue de Physique Appliquée* **15** (1980): 1261–1265.

CAS | Google Scholar

38 M. Russo, G. Iervolino, V. Vaiano, and V. Palma, "Non-Thermal Plasma Coupled With Catalyst for the Degradation of Water Pollutants: A Review," *Catalysts* **10** (2020): 1438, https://doi.org/10-3390/CATAL10121438.

CAS | Web of Science® | Google Scholar

39 N. Jiang, J. Hu, J. Li, K. Shang, N. Lu, and Y. Wu, "Plasma-Catalytic Degradation of Benzene over Ag-Ce Bimetallic Oxide Catalysts Using Hybrid Surface/Packed-Bed Discharge Plasmas," *Applied Catalysis, B: Environmental* **184** (2016): 355–363, https://doi.org/10.1016/J.APCATB.2015.11.044.

CAS | Web of Science® | Google Scholar

40 A. Bogaerts, X. Tu, J. C. Whitehead, et al., "The 2020 Plasma Catalysis Roadmap," *Journal of Physics D: Applied Physics* **53** (2020): 443001, https://doi.org/10.1088/1361-6463/ab9048.

CAS | Web of Science® | Google Scholar

41 J. H. Cho, S. H. An, T. S. Chang, and C. H. Shin, "Effect of an Alumina Phase on the Reductive Amination of 2-Propanol to Monoisopropylamine over Ni/Al2O3," *Catalysis Letters* **146** (2016): 811–819, http...

43 X. Huang, J. Liu, J. Chen, Y. Xu, and W. Shen, "Mechanistic Study of Selective Oxidation of Dimethyl Ether to Formaldehyde over Alumina-Supported Molybdenum Oxide Catalyst," *Catalysis Letters* **108** (2006): 79–86, https://doi.org/10.1007/s10562-006-0019-9.

CAS | Web of Science® | Google Scholar

44 D. Shi, H. Wang, L. Kovarik, et al., "Wo Supported on γ-Al2O3 With Different Morphologies as Model Catalysts for Alkanol Dehydration," *Journal of Catalysis* **363** (2018): 1–8, https://doi.org/10.1016/j.jcat.2018.04.004.

CAS | Google Scholar

45 T. P. Braga, A. N. Pinheiro, E. R. Leite, R. C. R. Santos, and A. Valentini, "Cu, Fe, or Ni Doped Molybdenum Oxide Supported on Al2O3 for the Oxidative Dehydrogenation of Ethylbenzene," *Chinese Journal of Catalysis* **36** (2015): 712–720, https://doi.org/10.1016/S18722067(14)-60313-2.

CAS | Web of Science® | Google Scholar

46 J. Wang, H. Yi, X. Tang, S. Zhao, and F. Gao, "Exceptional Adsorptive Capacity and Kinetic of γ-Al2O3 for Selective Adsorption of NO Assisted by Nonthermal Plasma," *Chemical Engineering Journal* **378** (2019): 122095.

CAS | Google Scholar

47 J. Hong, S. Prawer, and A. B. Murphy, "Plasma Catalysis as an Alternative Route for Ammonia Production: Status, Mechanisms, and Prospects for Progress," *ACS Sustainable Chemistry and Engineering* **6** (2018): 15–31, https://doi.org/10.1021/acssuschemeng.7b02381.

CAS | Web of Science® | Google Scholar

48 T. Mizushima, K. Matsumoto, H. Ohkita, and N. Kakuta, "Catalytic Effects of Metal-Loaded Membrane-Like Alumina Tubes on Ammonia Synthesis in Atmospheric Pressure Plasma by Dielectric Barrier Discharge," *Plasma Chemistry and Plasma Processing* **27** (2007): 1–11, https://doi.org/10.1007/S11090-006-9034-2/FIGURES/8.

CAS | Web of Science® | Google Scholar

49 M. Iwamoto, M. Akiyama, K. Aihara, and T. Deguchi, "Ammonia Synthesis on Wool-Like Au, Pt, Pd, Ag, or Cu Electrode Catalysts in Nonthermal Atmospheric-Pressure Plasma of N_2 and H_2," *ACS Catalysis* **7** (2017): 6924–6929, https://doi.org/10.1021/ACSCATAL.7B01624/-ASSET/IMAGES/CS-2017-01624J_M009.GIF.

CAS | Web of Science® | Google Scholar

50 J. Hong, M. Aramesh, O. Shimoni, et al., "Plasma Catalytic Synthesis of Ammonia Using Functionalized-Carbon Coatings in an Atmospheric-Pressure Non-Equilibrium Discharge," *Plasma Chemistry and Plasma Processing* **36** (2016): 917–940, https://doi.org/10.1007/S11090-016-9711-8/FIGURES/15.

CAS | Web of Science® | Google Scholar

51 A. Gómez-Ramírez, A. M. Montoro-Damas, J. Cotrino, R. M. Lambert, and A. R. González-Elipe, "About the Enhancement of Chemical Yield During the Atmospheric Plasma Synthesis of Ammonia in a Ferroelectric Packed Bed Reactor," *Plasma Processes and Polymers* **14** (2017), https://onlinelibrary.wiley.com/doi/10.1002/ppap.201600081.

CAS | Web of Science® | Google Scholar

54 P. Peng, Y. Cheng, R. Hatzenbeller, et al., "Ru-Based Multifunctional Mesoporous Catalyst for Low-Pressure and Non-Thermal Plasma Synthesis of Ammonia," *International Journal of Hydrogen Energy* **42** (2017): 19056–19066, https://doi.org/10.1016/J.IJHYDENE.2017.06.118.

CAS | Web of Science® | Google Scholar

55 L. Hollevoet, F. Jardali, Y. Gorbanev, J. Creel, A. Bogaerts, and J. A. Martens, "Towards Green Ammonia Synthesis Through Plasma-Driven Nitrogen Oxidation and Catalytic Reduction," *Angewandte Chemie International Edition* **59** (2020): 23825–23829.

CAS | PubMed | Web of Science® | Google Scholar

56 Y. Engelmann, K. van 't Veer, Y. Gorbanev, E. C. Neyts, W. F. Schneider, and A. Bogaerts, "Plasma Catalysis for Ammonia Synthesis: A Microkinetic Modeling Study on the Contributions of Eley-Rideal Reactions," *ACS Sustainable Chemistry and Engineering* **9** (2021): 13151–13163, https://doi.org/10.1021/acssuschemeng.1c02713.

CAS | Web of Science® | Google Scholar

57 A. Gicquel, S. Cavadias, and J. Amouroux, "Heterogeneous Catalysis in Low-Pressure Plasmas," *Journal of Physics D: Applied Physics* **19** (1986): 2013–2042.

CAS | Web of Science® | Google Scholar

58 E. N. Eremin, V. M. Belova, and A. N.: Mal'tsev, "Heterogeneous Catalytic Oxidation of Nitrogen in Glow-Discharge. III.1: 4 N Sub 2: O Sub 2 Mixture," *Zhurnal Fizicheskoi Khimii* **52** (1978): 1679–1682.

CAS | Google Scholar

59 V. M. Belova, E. N. Eremin, and A. N.: Mal'tsev, "Heterogeneous Catalytic Oxidation of Nitrogen in a Glow Discharge II 1: 1 Nitrogen-Oxygen Mixture," *Russian Journal of Physical Chemistry* **52** (1978): 968–970.

Google Scholar

60 B. S. Patil, N. Cherkasov, J. Lang, A. O. Ibhadon, V. Hessel, and Q. Wang, "Low Temperature Plasma-Catalytic NOx Synthesis in a Packed DBD Reactor: Effect of Support Materials and Supported Active Metal Oxides," *Applied Catalysis, B: Environmental* **194** (2016): 123–133.

CAS | Web of Science® | Google Scholar

61 F. Chang, W. Gao, J. Guo, and P. Chen, "Emerging Materials and Methods Toward Ammonia-Based Energy Storage and Conversion," *Advanced Materials* **33** (2021): 2005721, https://doi.org/10.1002/adma.202005721.

CAS | Web of Science® | Google Scholar

62 G. Akay, "Plasma Generating—Chemical Looping Catalyst Synthesis by Microwave Plasma Shock for Nitrogen Fixation From Air and Hydrogen Production From Water for Agriculture and Energy

CAS | Web of Science® | Google Scholar

65 T. Silva, N. Britun, T. Godfroid, and R. Snyders, "Optical Characterization of a Microwave Pulsed Discharge Used for Dissociation of CO2," *Plasma Sources Science and Technology* **23** (2014): 025009.

CAS | Web of Science® | Google Scholar

66 A. Goldman, L. R. Brown, W. G. Schoenfeld, et al., "Nitric Oxide Line Parameters: Review of 1996 HITRAN Update and New Results," *Journal of Quantitative Spectroscopy and Radiative Transfer* **60** (1998): 825–838.

CAS | Web of Science® | Google Scholar

67 H. W. Thompson and B. A. Green, "The Fundamental Vibration Band of Nitric Oxide," *Spectrochimica Acta* **8** (1956): 129–137.

CAS | Google Scholar

68 J. Ballard, W. B. Johnston, B. J. Kerridge, and J. J. Remedios, "Experimental Spectral Line Parameters in the 1-0 Band of Nitric Oxide," *Journal of Molecular Spectroscopy* **127** (1988): 70–82.

CAS | Web of Science® | Google Scholar

69 L. S. Rothman, I. E. Gordon, Y. Babikov, et al., "The HITRAN2012 Molecular Spectroscopic Database," *Journal of Quantitative Spectroscopy and Radiative Transfer* **130** (2013): 4–50, https://doi.org/10.1016/J.JQSRT.2013.07.002.

CAS | Web of Science® | Google Scholar

70 O. Samadi Bahnamiri, F. Manaigo, A. Chatterjee, R. Snyders, F. A. D'Isa, and N. Britun, "Investigation of Nitrogen Fixation in Low-Pressure Microwave Plasma via Rotational-Vibrational NO and N2kinetics," *Journal of Applied Physics* **133** (2023), https://doi.org/10.1063/5.0138298.

Google Scholar

71 O. S. Bahnamiri, C. Verheyen, R. Snyders, A. Bogaerts, and N. Britun, "Nitrogen Fixation in Pulsed Microwave Discharge Studied by Infrared Absorption Combined With Modelling," *Plasma Sources Science and Technology* **30** (2021): 065007, https://doi.org/10.1088/1361-6595/abff0e.

CAS | Web of Science® | Google Scholar

72 Y. B. Zeldvich, "The Oxidation of Nitrogen in Combustion and Explosions," *Journal of Acta Physicochimica.* **21** (1946): 577.

Google Scholar

73 P. Mehta, P. Barboun, D. B. Go, J. C. Hicks, and W. F. Schneider, "Catalysis Enabled by Plasma Activation of Strong Chemical Bonds: A Review," *ACS Energy Letters* **4** (2019): 1115–1133, https://doi.org/10.1021/acsenergylett.9b00263.

CAS | Web of Science® | Google Scholar

76 C. V. Chandran, C. E. A. Kirschhock, S. Radhakrishnan, F. Taulelle, J. A. Martens, and E. Breynaert, "Alumina: Discriminative Analysis Using 3D Correlation of Solid-State NMR Parameters," *Chemical Society Reviews* **48** (2019): 134–156, https://doi.org/10.1039/C8CS00321A.

CAS | PubMed | Web of Science® | Google Scholar

77 H. Dexpert, J. F. Larue, I. Mutin, B. Moraweck, Y. Bertaud, and A. Renouprez, "Thermal Transformation of Transition Aluminas," *JOM* **37** (1985): 17–21, https://doi.org/10.1007/-BF03258733/METRICS.

CAS | Google Scholar

78 K. Kaunisto, J. Lagerbom, M. Honkanen, et al., "Evolution of Alumina Phase Structure in Thermal Plasma Processing," *Ceramics International* **49** (2023): 21346–21354, https://doi.org/10.1016/J.CERAMINT.2023.-03.263.

CAS | Web of Science® | Google Scholar

79 I. Levin and D. Brandon, "Metastable Alumina Polymorphs: Crystal Structures and Transition Sequences," *Journal of the American Ceramic Society* **81** (1998): 1995–2012, https://doi.org/10.1111/J.1151-2916.1998.TB02581.X.

CAS | Web of Science® | Google Scholar

80 S. Dahl, A. Logadottir, C. J. H. Jacobsen, and J. K. Nørskov, "Electronic Factors in Catalysis: The Volcano Curve and the Effect of Promotion in Catalytic Ammonia Synthesis," *Applied Catalysis, A: General* **222** (2001): 19–29, https://doi.org/10.1016/S0926-860X(01)00826-2.

CAS | Web of Science® | Google Scholar

81 C. J. H. Jacobsen, S. Dahl, B. S. Clausen, S. Bahn, A. Logadottir, and J. K. Nørskov, "Catalyst Design by Interpolation in the Periodic Table: Bimetallic Ammonia Synthesis Catalysts," *Journal of the American Chemical Society* **123** (2001): 8404–8405, https://doi.org/10.1021/JA010963D.

CAS | PubMed | Web of Science® | Google Scholar

82 L. Kovarik, M. Bowden, and J. Szanyi: High Temperature Transition Aluminas in δ-Al2O3/θ-Al2O3 Stability Range: Review, (2021).

Google Scholar

83 P. K. Kiyohara, H. Souza Santos, A. C. V. Coelho, P. De, and S. Santos: Structure, Surface Area and Morphology of Aluminas From Thermal Decomposition of Al(OH)(CH 3 COO) 2 Crystals. (2000).

Google Scholar

84 Z. Nie and Y. Lin. Fabrication of Porous Alumina Ceramics With Corn Starch in an Easy and Low-cost Way (2016), https://www.ceramics-silikaty.cz/index.phppage=cs_detail_doi&id=77.

Google Scholar

87 R. B. Watson and U. S. Ozkan, "Mo Loading Effects over Mo/Si: Ti Catalysts in the Oxidative Dehydrogenation of Ethane," *Journal of Catalysis* **208** (2002): 124–138.

CAS | Web of Science® | Google Scholar

88 K. Chen, S. Xie, A. T. Bell, and E. Iglesia, "Structure and Properties of Oxidative Dehydrogenation Catalysts Based on MoO_3/Al_2O_3," *Journal of Catalysis* **198** (2001): 232–242.

CAS | Web of Science® | Google Scholar

89 Y. Matsumoto and R. Shimanouchi, " Synthesis of Al2(MoO4)3 by Two Distinct Processes, Hydrothermal Reaction and Solid-State Reaction." *Procedia Engineering* (Elsevier Ltd, 2016), 158–162.

Google Scholar

90 A. C. Bararaj, D. B. Mathi, N. R. Yogamalar, and A. C. Bose, "Structural Evolution and Phase Transition of [NH4]6Mo7O24.4H2O to 2D Layered Moo3-X," *Materials Research Express* **2** (2015), https://doi.org/10.1088/2053-1591/2/5/055004.

Google Scholar

Download PDF